

Supplementary information

Cation disorder and octahedral distortion control of internal electric field, band bending and carrier lifetime in Aurivillius perovskite solid-solutions for enhanced photocatalytic activity

Jaideep Malik,^a Shubham Kumar, ^aPriya Srivastava,^b Monojit Bag^{b,c} and Tapas Kumar

Manda^{a,c,*}

^aDepartment of Chemistry, ^bDepartment of Physics & ^cCentre of Nanotechnology, Indian Institute of Technology Roorkee, Roorkee – 247 667, India.

Corresponding author e-mail: tapas.mandal@cy.iitr.ac.in.

Table S1 Chemical compositions and synthesis conditions for five-layer Aurivillius phases

Sl. No.	Chemical composition	Synthesis condition
1.	$\text{Bi}_5\text{SrTi}_4\text{FeO}_{18}$	780 °C/2 h; 1000 °C/2 h in air
2.	$\text{Bi}_{5.25}\text{Sr}_{0.75}\text{Ti}_{3.75}\text{Fe}_{1.25}\text{O}_{18}$	780 °C/2 h; 1000 °C/2 h in air
3.	$\text{Bi}_{5.5}\text{Sr}_{0.5}\text{Ti}_{3.5}\text{Fe}_{1.5}\text{O}_{18}$	780°C/2 h; 1000 °C/2 + 2 h in air
4.	$\text{Bi}_{5.75}\text{Sr}_{0.25}\text{Ti}_{3.25}\text{Fe}_{1.75}\text{O}_{18}$	780°C/2 h; 1000 °C/2 + 2 h in air
5.	$\text{Bi}_6\text{Ti}_3\text{Fe}_2\text{O}_{18}$	780°C/2 h; 1000 °C/6 h in air

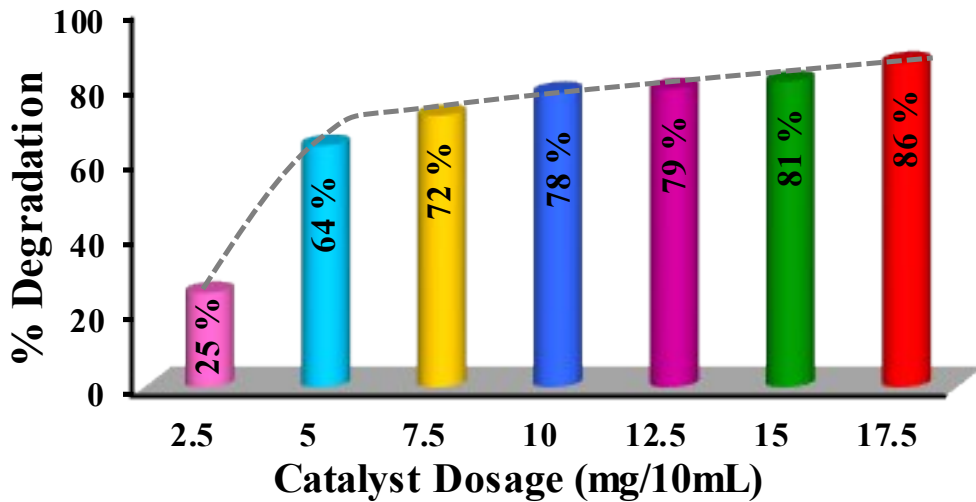


Fig. S1 Effect of catalyst dosage for degradation of RhB at pH 2 over $\text{Bi}_{5.75}\text{Sr}_{0.25}\text{Ti}_{3.25}\text{Fe}_{1.75}\text{O}_{18}$ under MP Mercury Vapor Lamp for 10 min.

Table S2 Lattice parameters and bandgap energies of $\text{Bi}_{6-x}\text{Sr}_x\text{Ti}_{3+x}\text{Fe}_{2-x}\text{O}_{18}$ ($x = 1.0, 0.75, 0.5, 0.25$).

Compounds	Lattice parameters (Å)			Bandgap (eV)	
	<i>a</i>	<i>b</i>	<i>c</i>	$E_g(1)$	$E_g(2)$
$\text{Bi}_5\text{SrTi}_4\text{FeO}_{18}$	5.475(2)	5.484(3)	49.34(1)	2.18	2.74
$\text{Bi}_{5.25}\text{Sr}_{0.75}\text{Ti}_{3.75}\text{Fe}_{1.25}\text{O}_{18}$	5.462(0)	5.455(1)	49.18(0)	2.13	2.66
$\text{Bi}_{5.5}\text{Sr}_{0.5}\text{Ti}_{3.5}\text{Fe}_{1.5}\text{O}_{18}$	5.462(0)	5.454(0)	49.30(0)	2.11	2.64
$\text{Bi}_{5.75}\text{Sr}_{0.25}\text{Ti}_{3.25}\text{Fe}_{1.75}\text{O}_{18}$	5.470(1)	5.460(1)	49.38(1)	2.08	2.62

Table S3 Atomic position, site occupancy and thermal parameters of $\text{Bi}_{5.75}\text{Sr}_{0.25}\text{Ti}_{3.25}\text{Fe}_{1.75}\text{O}_{18}$

Atom	<i>x</i>	<i>y</i>	<i>z</i>	B _{iso}	occ.
Bi(1)	0.5539(45)	0	0.72376(7)	1.32	2
Bi(2)/Sr(2)	0.5516(34)	0	0.54240(9)	1.32	1.875/0.125
Bi(3)/Sr(3)	0.5502(44)	0	0.62956(8)	1.32	1.875/0.125
Ti(1)/Fe(1)	0.5131(57)	0	0.8336	0.83	1.625/0.375
Ti(2)/Fe(2)	0.5083(34)	0	0.9171(21)	0.83	1.625/0.375
Fe(3)	0.5	0	0	0.83	1
O(1)	0.25	0.75	0	3.1	2
O(2)	0.75	0.25	0.25	3.1	2
O(3)	0.5	0	0.7987(10)	3.1	2
O(4)	0.5	0	0.8821(10)	3.1	2
O(5)	0.5	0	0.96332(9)	3.1	2
O(6)	0.25	0.25	0.42504(8)	3.1	4
O(7)	0.25	0.25	0.33941(9)	3.1	4

Space group $F2mm$, $a = 5.4595(3)$, $b = 5.4396(3)$, $c = 49.193(3)$ Å, $R_{\text{Bragg}} = 3.1\%$, $R_F = 1.8\%$, $R_p = 6.1\%$, $R_{wp} = 7.7\%$, and $\chi^2 = 1.6$.

Atom	<i>x</i>	<i>y</i>	<i>z</i>	B _{iso}	occ.
Bi(1)	0.5563(3)	0	0.7237(1)	1.32	2
Bi(2)/Sr(2)	0.5396(3)	0	0.5426(1)	1.32	1.75/0.25
Bi(3)/Sr(3)	0.5420(3)	0	0.6297(1)	1.32	1.75/0.25
Ti(1)/Fe(1)	0.5094(6)	0	0.8323	0.83	1.75/0.25
Ti(2)/Fe(2)	0.4923(4)	0	0.9167(3)	0.83	1.75/0.25
Fe(3)	0.5	0	0	0.83	1
O(1)	0.25	0.75	0	3.1	2
O(2)	0.75	0.25	0.25	3.1	2
O(3)	0.5	0	0.7975(1)	3.1	2
O(4)	0.5	0	0.8816(1)	3.1	2
O(5)	0.5	0	0.9641(1)	3.1	2
O(6)	0.25	0.25	0.4235(7)	3.1	4
O(7)	0.25	0.25	0.3394(9)	3.1	4

Table S4 Atomic position, site occupancy and thermal parameters of $\text{Bi}_{5.5}\text{Sr}_{0.5}\text{Ti}_{3.5}\text{Fe}_{1.5}\text{O}_{18}$

Space group $F2mm$, $a = 5.4582(3)$, $b = 5.4412(3)$, $c = 49.147(2)$ Å, $R_{\text{Bragg}} = 3.1\%$, $R_F = 2.0\%$, $R_p = 6.7\%$, $R_{\text{wp}} = 8.4\%$, and $\chi^2 = 1.5$.

Atom	x	y	z	B_{iso}	Occ.
Bi(1)	0.5467(2)	0	0.7242(1)	1.32	2
Bi(2)/Sr(2)	0.5424(2)	0	0.5423(1)	1.32	1.625/0.375
Bi(3)/Sr(3)	0.5402(2)	0	0.6297(1)	1.32	1.625/0.375
Ti(1)/Fe(1)	0.5047(3)	0	0.8341	0.83	1.875/0.125
Ti(2)/Fe(2)	0.5164(3)	0	0.9171(2)	0.83	1.875/0.125
Fe(3)	0.5	0	0	0.83	1
O(1)	0.25	0.75	0	3.1	2
O(2)	0.75	0.25	0.25	3.1	2
O(3)	0.5	0	0.7998(6)	3.1	2
O(4)	0.5	0	0.8806(6)	3.1	2
O(5)	0.5	0	0.9635(3)	3.1	2
O(6)	0.25	0.25	0.4202(4)	3.1	4
O(7)	0.25	0.25	0.3444(1)	3.1	4

Table S5 Atomic position, site occupancy and thermal parameters of $\text{Bi}_{5.25}\text{Sr}_{0.75}\text{Ti}_{3.75}\text{Fe}_{1.25}\text{O}_{18}$

Space group $F2mm$, $a = 5.4737(1)$, $b = 5.4566(1)$, $c = 49.197(1)$ Å, $R_{\text{Bragg}} = 2.4\%$, $R_F = 2.2\%$, $R_p = 3.0\%$, $R_{\text{wp}} = 3.8\%$, and $\chi^2 = 2.9$.

Rietveld refinement

To obtain the lowest value of χ^2 with good fitting, all the parameters were refined one by one systematically, except the thermal and positional parameters of atoms present at general positions. However, to reach convergence Ti1 coordinates are kept fixed in all the refinements.⁵⁷ The refined atomic positions, occupancies and thermal factors for $\text{Bi}_{6-x}\text{Sr}_x\text{Ti}_{3+x}\text{Fe}_{2-x}\text{O}_{18}$ ($x = 0.75$ & 0.5) are given in Tables S3 and S4 in the Supporting Information. Generally, the octahedra are highly distorted at the terminal position (see bond distances given later) while the octahedral distortion

decreases as one moves toward the central layer due to the second-order Jahn-Teller effect of d⁰ cations (Ti⁴⁺ in this case). The detail analysis of octahedral distortion and distortion parameters are given later.

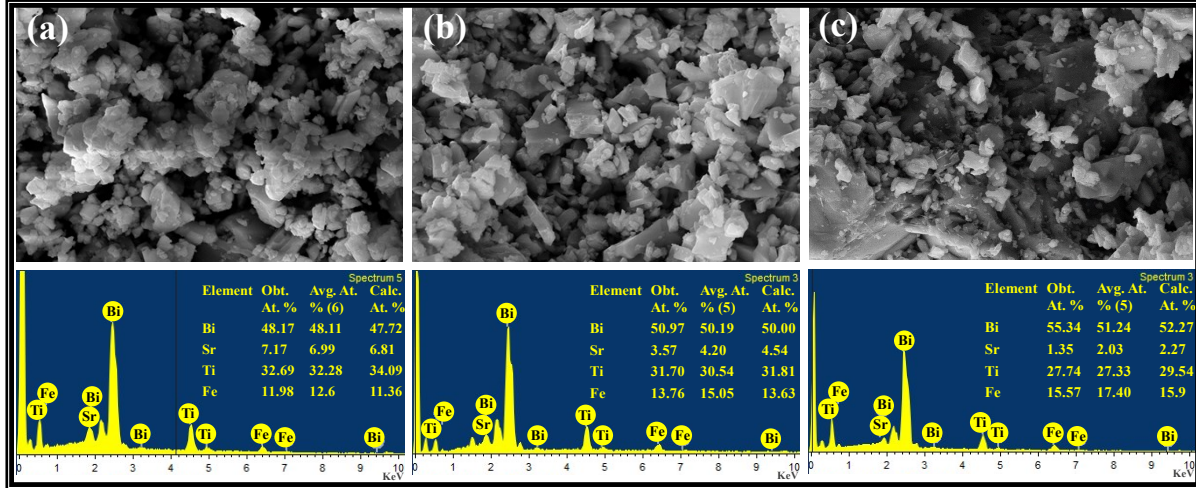


Fig. S2 FE-SEM images and corresponding EDS spectra of (a) Bi_{5.25}Sr_{0.75}Ti_{3.75}Fe_{1.25}O₁₈, (b) Bi_{5.5}Sr_{0.5}Ti_{3.5}Fe_{1.5}O₁₈ and (c) Bi_{5.75}Sr_{0.25}Ti_{3.25}Fe_{1.75}O₁₈.

Estimation of bandgap for Bi_{6-x}Sr_xTi_{3+x}Fe_{2-x}O₁₈ ($x = 1.0, 0.75, 0.5, 0.25, 0.0$)

The obtained reflectance data were converted to absorption terms by using Kubelka–Munk (K–M) theory.

$$F(R_\infty) = (1 - R_\infty)^2 / 2R_\infty \quad (1)$$

where, R_∞ is reflectance of the sample and $F(R_\infty)$ is the K–M function. The band gap (E_g) of the samples was determined from Tauc plots using the following equation.

$$(\alpha h\nu)^{1/n} = A(h\nu - E_g) \quad (2)$$

where, α is the absorption coefficient, $h\nu$ is the incident light frequency, A is the proportionality constant, E_g is the band gap of the compound and ‘ n ’ in the exponent signifies the nature of

electronic transition; for direct transition, $n = \frac{1}{2}$ and for indirect transition, $n = 2$. An extrapolation of steep linear part of the $(\alpha h\nu)^{1/n}$ verses $h\nu$ (eV) plot to the energy axis was employed for the estimation of band gaps.

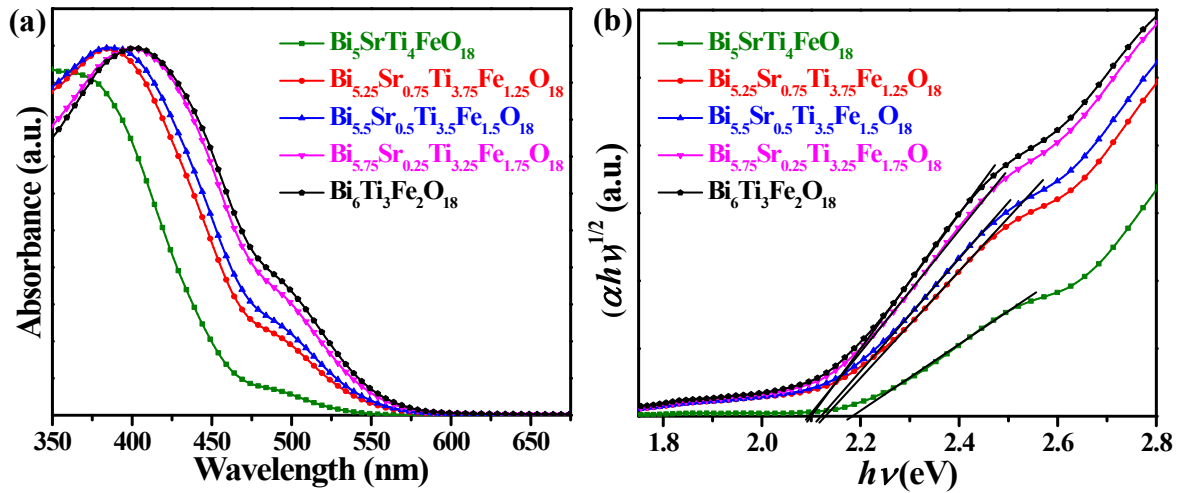


Fig. S3 (a) UV-Vis DRS of $\text{Bi}_{6-x}\text{Sr}_x\text{Ti}_{3+x}\text{Fe}_{2-x}\text{O}_{18}$ ($x = 1 - 0$) and corresponding (b) Tauc plots.

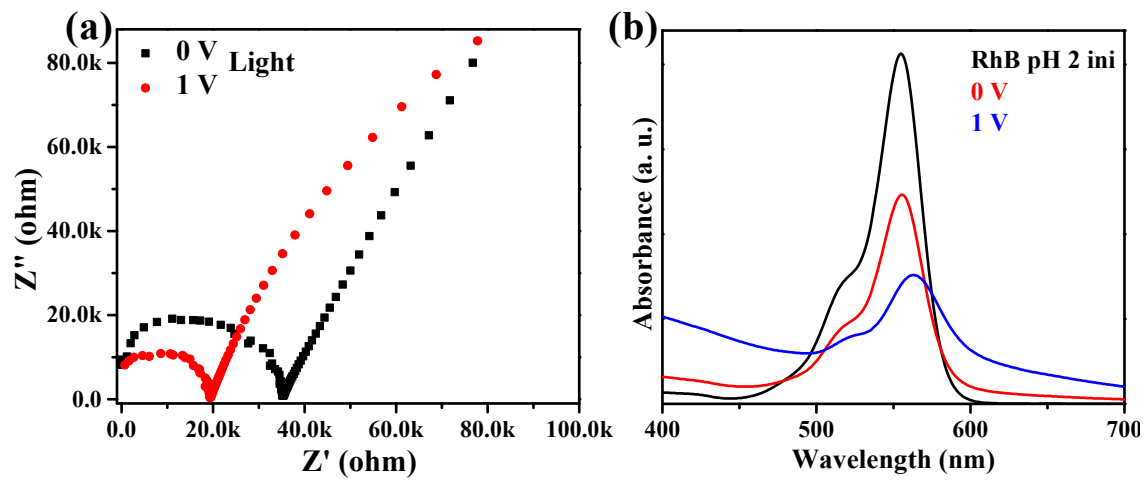


Fig. S4 (a) EIS Nyquist plots of $\text{Bi}_{5.75}\text{Sr}_{0.25}\text{Ti}_{3.25}\text{Fe}_{1.75}\text{O}_{18}$ under visible light illumination at 0 (black) and 1 V (red) bias and (b) Photocatalytic activity of $\text{Bi}_{5.75}\text{Sr}_{0.25}\text{Ti}_{3.25}\text{Fe}_{1.75}\text{O}_{18}$ after 5 minutes of visible light irradiation at 0 (red) and 1 V (blue) bias.

Fitting and analysis of impedance spectroscopy data on application of bias voltage

As already discussed earlier in the article that the photocatalytic activity of the photocatalyst is augmented on the application of external applied bias. The same is true for $\text{Bi}_{5.25}\text{Sr}_{0.75}\text{Ti}_{3.75}\text{Fe}_{1.25}\text{O}_{18}$ and $\text{Bi}_6\text{Ti}_2\text{Fe}_2\text{O}_{18}$. It can be seen from the impedance feature of the photocatalyst device under illumination on application of external bias in the Figures S5 & S7 below. On application of the voltage, the value of R_{CT} decreases leading to the higher photocatalytic activity. A conventional R-C model with Warburg component is used for the fitting of the impedance data. It can also be seen from the fitting parameters that the value of R_{CT} decreases on application of external potential. Hence, it can be concluded that these materials have potential for application in photoelectrochemical (PEC) devices.

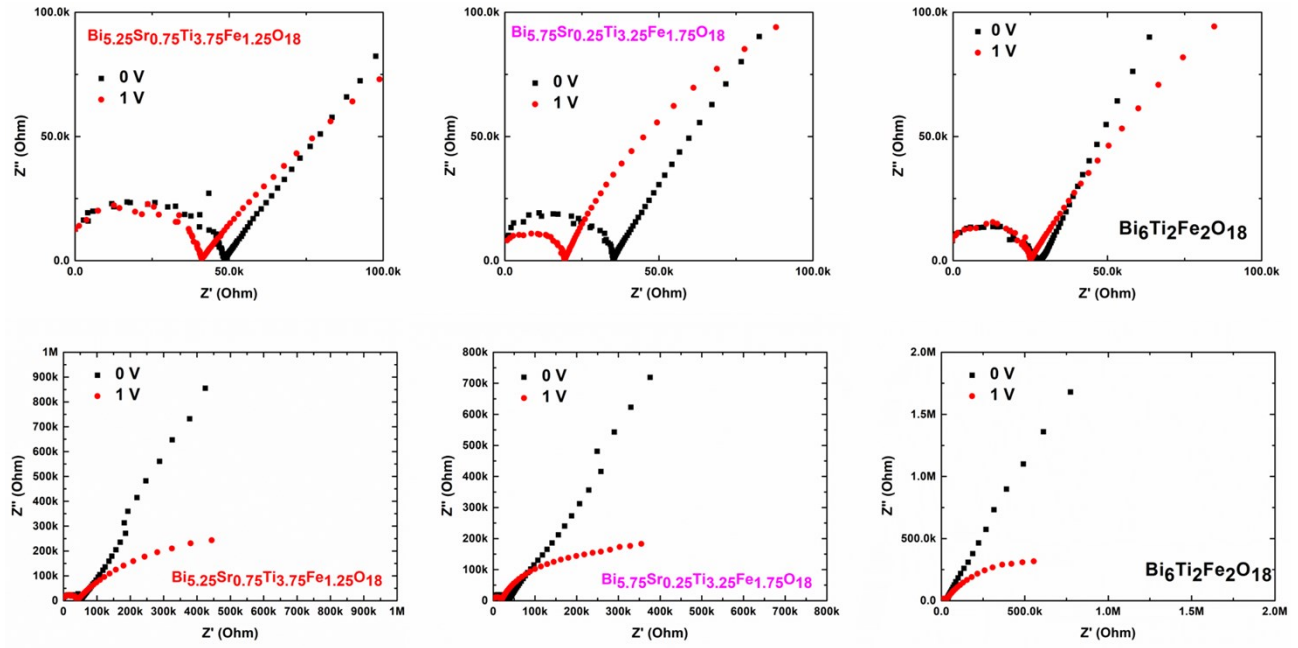


Fig. S5 EIS Nyquist plot of the photocatalysts under illumination on application of an external bias (top panel shows the expanded view of the bottom panel data).

The model used for the fitting of above Nyquist plots is shown in the Figure S6 below. Here, R_s is the series resistance due to the external circuit, R_{CT} is the charge transfer resistance, C_{dl} is the double layer capacitance formed due to the accumulation of ions at the solid-liquid interface and W is the Warburg component accounting for the mass transfer at the interface. The fitting parameters are given in the Table S4. Figure S7 shows the experimental and fitted impedance data. The low quality of fitting especially at low frequencies suggests that there are more kinetic processes going on at the interface including ion transport and charge transfer. However, the model is fitting pretty well at higher frequencies. More components corresponding to each of these processes are needed to be added to the equivalent circuit to get the exact fitting, which is out of the scope of this article.

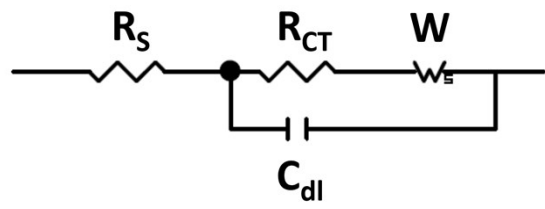


Fig. S6 Equivalent circuit used for fitting the impedance spectroscopy data.

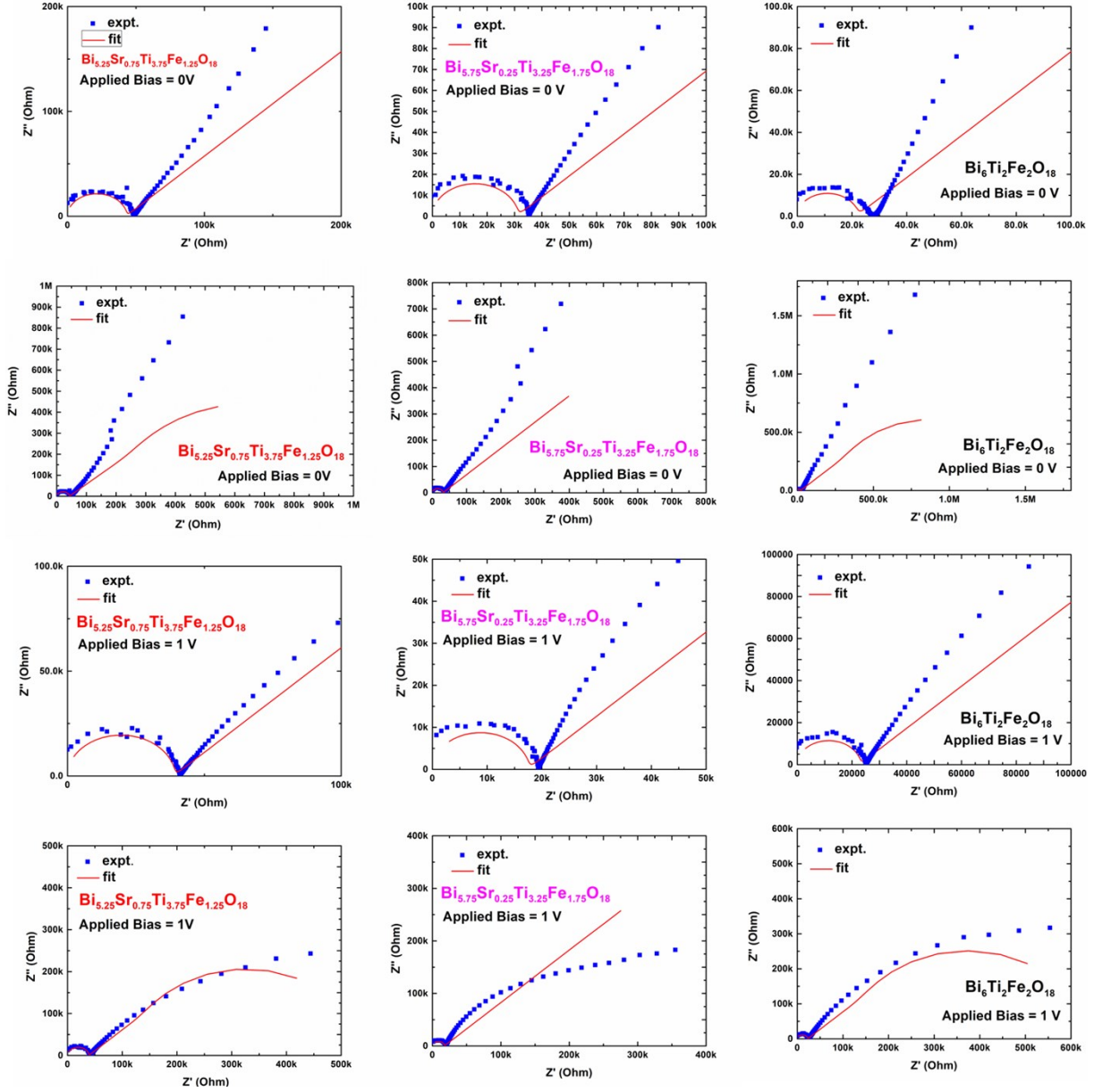


Fig. S7 Experimental impedance data and simulated fitting of the photocatalysts under illumination and at 0 and 1V bias (top panel shows the expanded view of the bottom panel data).

Table S6 Fitting parameters of the impedance data using the model mentioned above under illumination.

Applied								
Bias (V)	Chi-Sqr	Sum-Sqr	R _S (+)	R _{CT} (+)	W-R(+)	W-T(+)	W-P(X)	C _{dI} (+)
Bi_{5.25}Sr_{0.75}Ti_{3.75}Fe_{1.25}O₁₈								
0	0.096837	20.045	2.84E-06	42665	1.06E+06	5.332	0.5	1.68E-11
1	0.033505	6.3994	6.69E-08	38789	4.94E+05	2.479	0.5	1.61E-11
Bi_{5.75}Sr_{0.25}Ti_{3.25}Fe_{1.75}O₁₈								
0	0.1023	21.176	6.69E-08	30786	3.24E+06	62	0.5	1.92E-11
1	0.077772	16.099	6.69E-08	17353	1.76E+06	37.01	0.5	1.96E-11
Bi₆Ti₂Fe₂O₁₈								
0	0.1972	37.665	2.84E-06	21528	1.46E+06	4.446	0.5	1.89E-11
1	0.064871	12.39	2.84E-06	22659	6.03E+05	2.255	0.5	1.79E-11

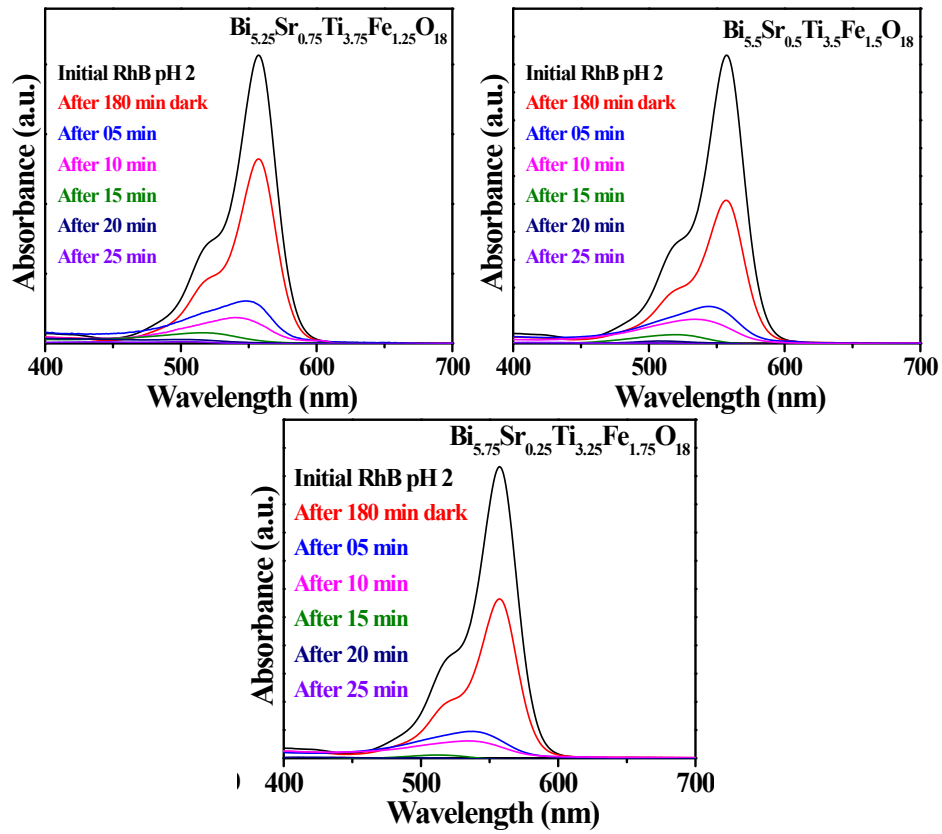


Fig. S8 UV-Vis absorption spectra of RhB degradation over (a) $\text{Bi}_{5.25}\text{Sr}_{0.75}\text{Ti}_{3.75}\text{Fe}_{1.25}\text{O}_{18}$, (b) $\text{Bi}_{5.5}\text{Sr}_{0.5}\text{Ti}_{3.5}\text{Fe}_{1.5}\text{O}_{18}$ and (c) $\text{Bi}_{5.75}\text{Sr}_{0.25}\text{Ti}_{3.25}\text{Fe}_{1.75}\text{O}_{18}$ at pH 2.

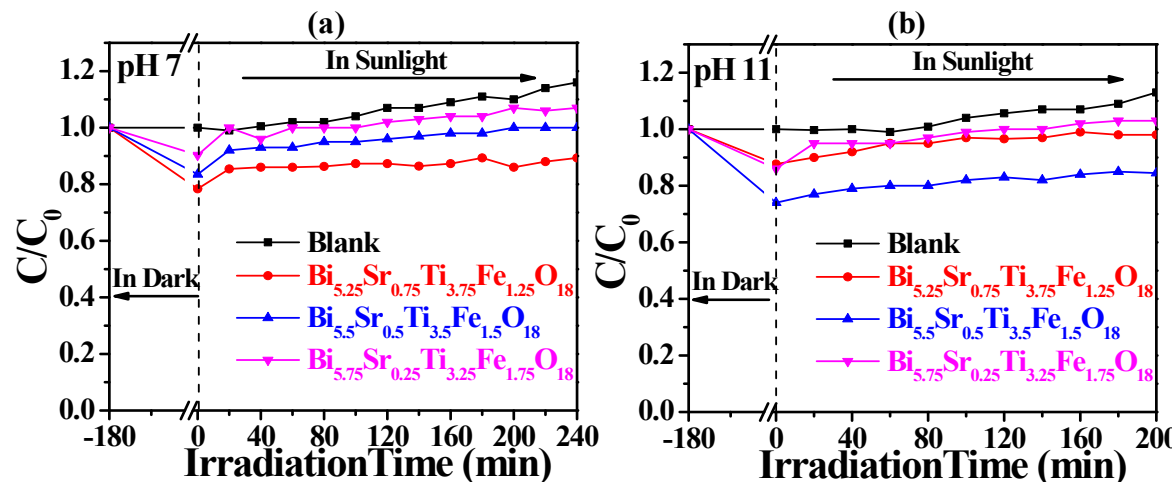


Fig. S9 Photocatalytic degradation of RhB over $\text{Bi}_{6-x}\text{Sr}_x\text{Ti}_{3+x}\text{Fe}_{2-x}\text{O}_{18}$ ($x = 0.75, 0.5, 0.25$) at (a) pH 7 and (b) pH 11 under sunlight irradiation.

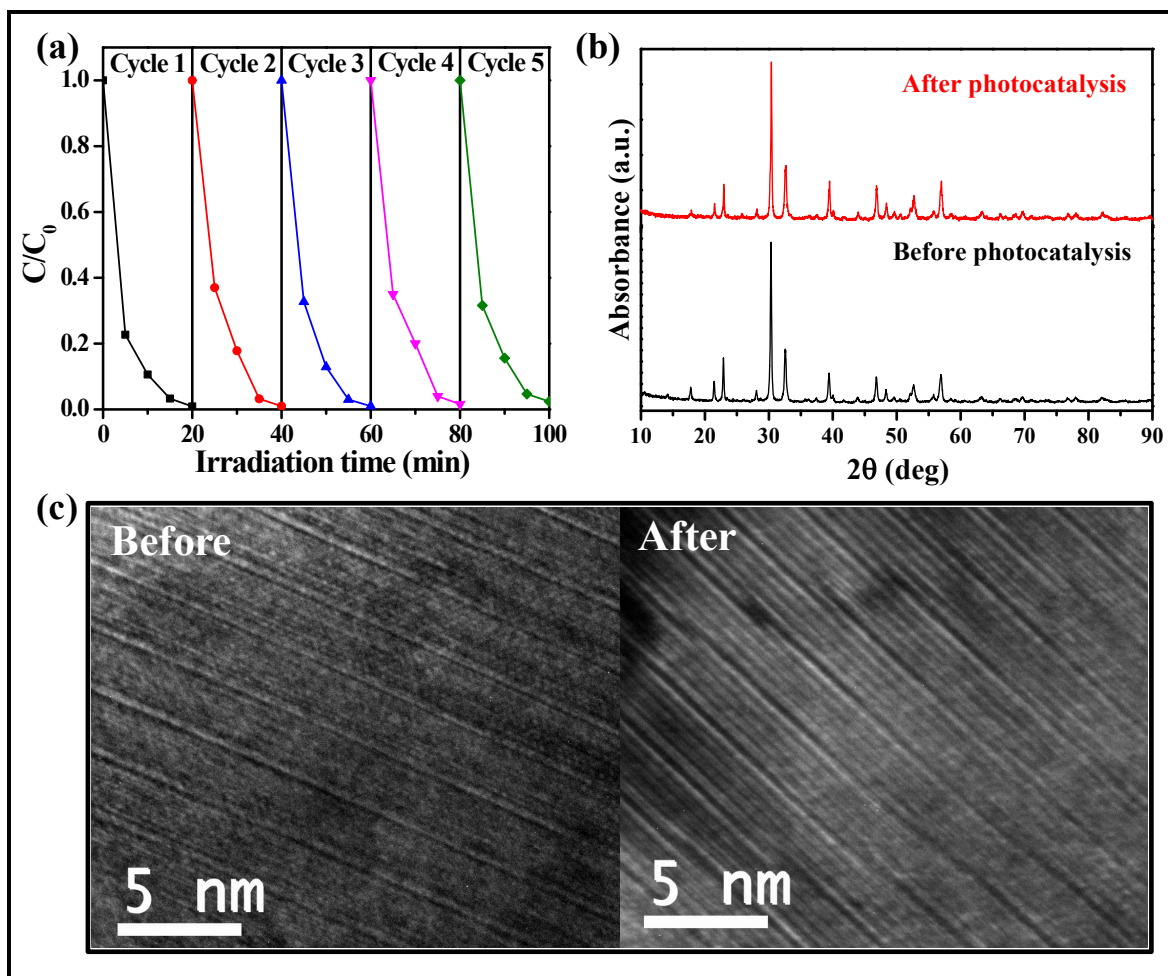


Fig. S10 (a) Photocatalytic cycle study of RhB degradation and (b) PXRD patterns recorded before and after five cyclic runs of RhB degradation over $\text{Bi}_{5.75}\text{Sr}_{0.25}\text{Ti}_{3.25}\text{Fe}_{1.75}\text{O}_{18}$. (c) HR-TEM images of $\text{Bi}_{5.75}\text{Sr}_{0.25}\text{Ti}_{3.25}\text{Fe}_{1.75}\text{O}_{18}$ before and after photocatalytic cycle study.

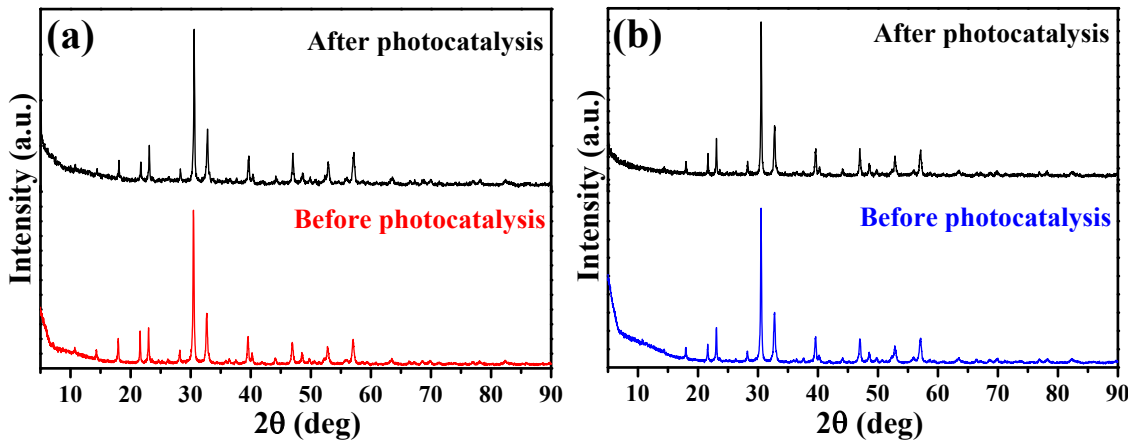


Fig. S11 PXRD patterns of (a) $\text{Bi}_{5.25}\text{Sr}_{0.75}\text{Ti}_{3.75}\text{Fe}_{1.25}\text{O}_{18}$ and (b) $\text{Bi}_{5.5}\text{Sr}_{0.5}\text{Ti}_{3.5}\text{Fe}_{1.5}\text{O}_{18}$ before and after the photocatalytic degradation of RhB.

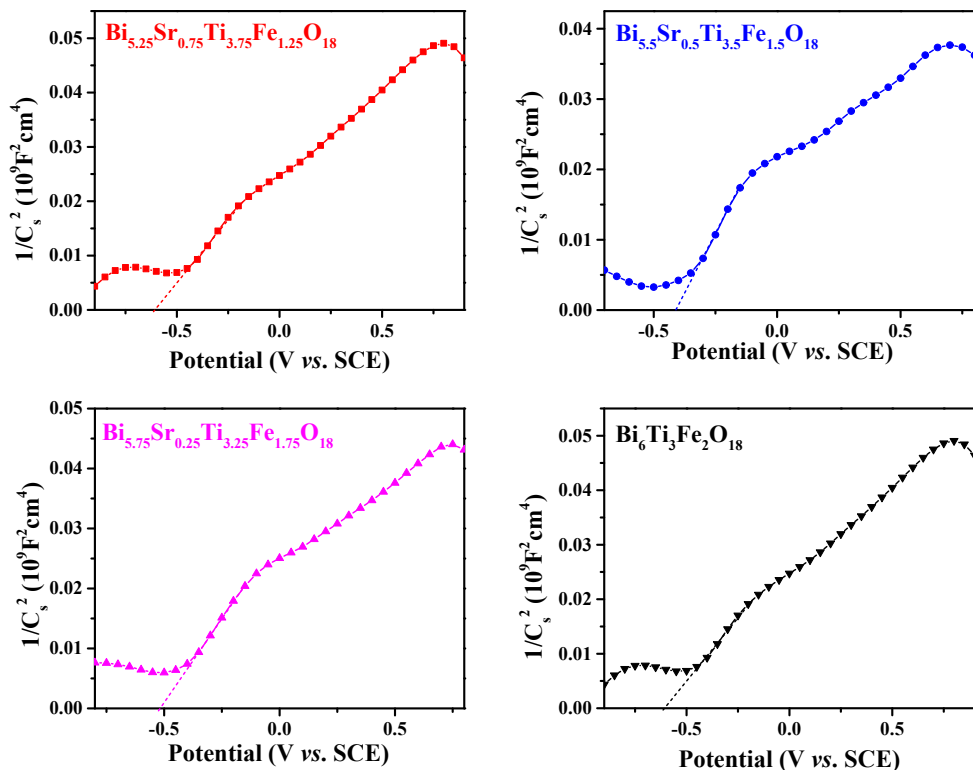


Fig. S12 Mott–Schottky plots of $\text{Bi}_{6-x}\text{Sr}_x\text{Ti}_{3+x}\text{Fe}_{2-x}\text{O}_{18}$ ($x = 0.75, 0.5, 0.25$ & 0.0).

Table S7 Flat-band potentials of $\text{Bi}_{6-x}\text{Sr}_x\text{Ti}_{3+x}\text{Fe}_{2-x}\text{O}_{18}$ ($x = 0.75, 0.5, 0.25 \& 0.0$) calculated from Mott-Schottky plots

Sl. No.	Sample name	Bandgap	E_{fb} (SCE)	E_{fb} (NHE)
		(eV)	(eV)	(eV)
1.	$\text{Bi}_{5.25}\text{Sr}_{0.75}\text{Ti}_{3.75}\text{Fe}_{1.25}\text{O}_{18}$	2.13	-0.575	-0.333
2.	$\text{Bi}_{5.5}\text{Sr}_{0.5}\text{Ti}_{3.5}\text{Fe}_{1.5}\text{O}_{18}$	2.11	-0.398	-0.156
3.	$\text{Bi}_{5.75}\text{Sr}_{0.25}\text{Ti}_{3.25}\text{Fe}_{1.75}\text{O}_{18}$	2.08	-0.511	-0.269
4.	$\text{Bi}_6\text{Ti}_3\text{Fe}_2\text{O}_{18}$	2.08	-0.472	-0.230

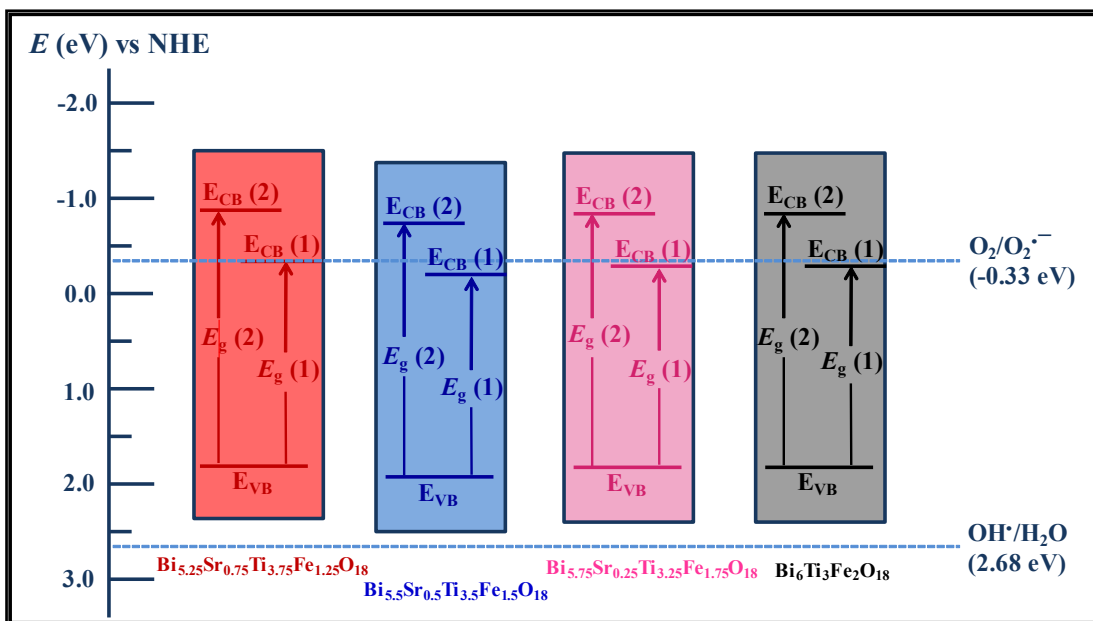


Fig. S13 Energy level diagrams of $\text{Bi}_{5.25}\text{Sr}_{0.75}\text{Ti}_{3.75}\text{Fe}_{1.25}\text{O}_{18}$, $\text{Bi}_{5.5}\text{Sr}_{0.5}\text{Ti}_{3.5}\text{Fe}_{1.5}\text{O}_{18}$, $\text{Bi}_{5.75}\text{Sr}_{0.25}\text{Ti}_{3.25}\text{Fe}_{1.75}\text{O}_{18}$ and $\text{Bi}_6\text{Ti}_3\text{Fe}_2\text{O}_{18}$ with their VB and CB edges determined from the Mott–Schottky plots and the respective band gaps.

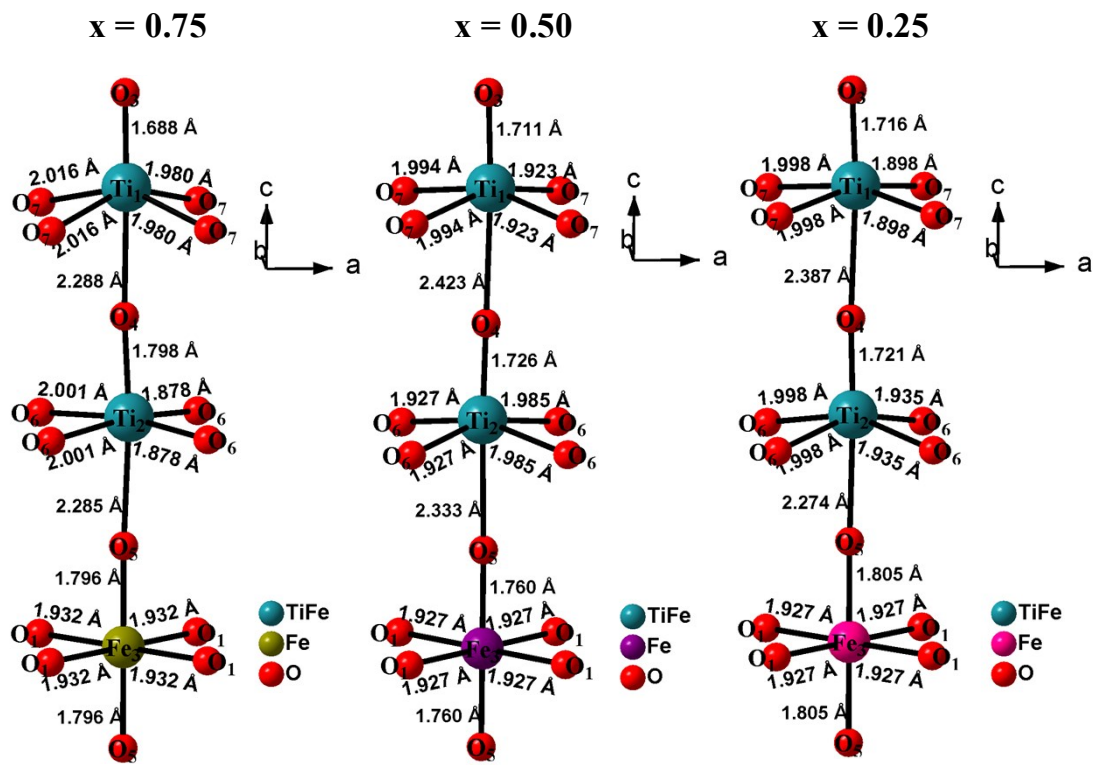


Fig. S14 Axial and equatorial bond distances of terminal, pre-terminal and central octahedra of $\text{Bi}_6\text{-}x\text{Sr}_x\text{Ti}_{3+x}\text{Fe}_{2-x}\text{O}_{18}$ ($x = 0.75, 0.5 \& 0.25$).

Table S8 Octahedral distortion parameters for $\text{Bi}_{5.25}\text{Sr}_{0.75}\text{Ti}_{3.75}\text{Fe}_{1.25}\text{O}_{18}$, $\text{Bi}_{5.5}\text{Sr}_{0.5}\text{Ti}_{3.5}\text{Fe}_{1.5}\text{O}_{18}$ and $\text{Bi}_{5.75}\text{Sr}_{0.25}\text{Ti}_{3.25}\text{Fe}_{1.75}\text{O}_{18}$

Compound	Octahedral distortion (Δ_o)			Axial octahedral distortion (Δ_{ax})		
	terminal	pre-terminal	central	terminal	pre-terminal	central
$\text{Bi}_{5.25}\text{Sr}_{0.75}\text{Ti}_{3.75}\text{Fe}_{1.25}\text{O}_{18}$	0.0076	0.0063	0.0011	0.0226	0.0164	0.0023
$\text{Bi}_{5.5}\text{Sr}_{0.5}\text{Ti}_{3.5}\text{Fe}_{1.5}\text{O}_{18}$	0.0115	0.0083	0.0017	0.0331	0.0241	0.0035
$\text{Bi}_{5.75}\text{Sr}_{0.25}\text{Ti}_{3.25}\text{Fe}_{1.75}\text{O}_{18}$	0.0106	0.0067	0.0009	0.0298	0.01967	0.0018

Table S9 Final R-factors and chi² for Bi_{6-x}Sr_xTi_{3+x}Fe_{2-x}O₁₈ ($x = 0.75, 0.50 \text{ & } 0.25$) on changing amount of Sr (%) in the Bi₂O₂ layer

% Sr in Bi ₂ O ₂ layer	chi ²	R _p	R _{wp}	R _{Bragg}	R _F
Bi_{5.25}Sr_{0.75}Ti_{3.75}Fe_{1.25}O₁₈					
0	2.90	2.99	3.80	2.41	2.18
10%	2.66	2.89	3.64	2.26	2.09
20%	2.50	2.82	3.53	2.16	2.04
30%	2.41	2.76	3.47	2.08	1.995
35%	2.39	2.75	3.45	2.04	1.975
40%	2.39	2.74	3.45	2.01	1.96
45%	2.40	2.75	3.46	1.99	1.95
50%	2.42	2.76	3.48	1.97	1.94
Bi_{5.5}Sr_{0.5}Ti_{3.5}Fe_{1.5}O₁₈					
0	1.44	6.61	8.30	2.92	1.93
10%	1.43	6.59	8.27	2.86	1.83
15%	1.43	6.58	8.26	2.85	1.88
20%	1.43	6.58	8.26	2.86	1.85
25%	1.43	6.59	8.26	2.90	1.856
50%	1.45	6.65	8.32	3.11	1.825
Bi_{5.75}Sr_{0.25}Ti_{3.25}Fe_{1.75}O₁₈					
0	1.56	6.05	7.67	3.077	1.81
5%	1.55	6.04	7.65	3.04	1.80
10%	1.54	6.03	7.63	3.01	1.78
20%	1.53	6.01	7.61	2.96	1.75
30%	1.52	5.98	7.57	2.91	1.73
40%	1.51	5.96	7.55	2.87	1.71
50%	1.50	5.95	7.54	2.83	1.69

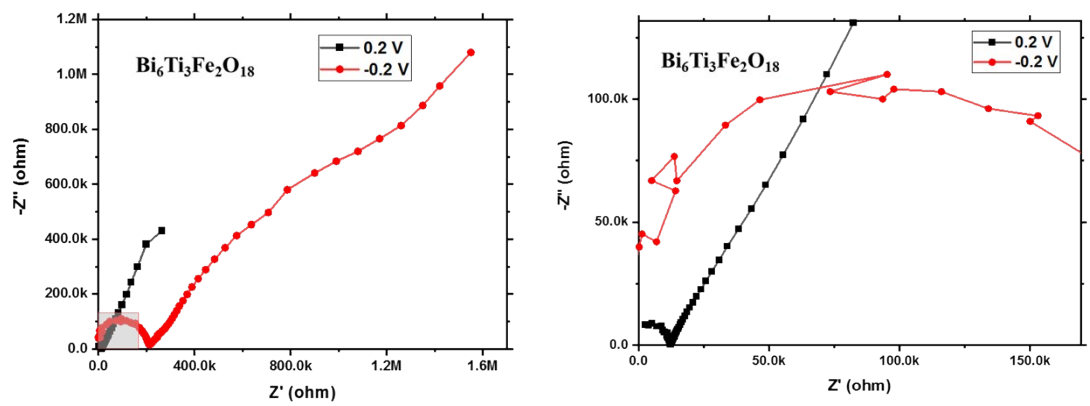


Fig. S15 The impedance data of $\text{Bi}_6\text{Ti}_3\text{Fe}_2\text{O}_{18}$ at ocp ($\sim -0.2 \text{ V}$) and at $+0.2 \text{ V}$.